the FEBS Journal

A modelling–experimental approach reveals insulin receptor substrate (IRS)-dependent regulation of adenosine monosphosphate-dependent kinase (AMPK) by insulin

Annika G. Sonntag[1,*], Piero Dalle Pezze[2,3,*], Daryl P. Shanley[2,3] and Kathrin Thedieck[1,4,5]

1 Bioinformatics and Molecular Genetics (Faculty of Biology), Institute for Biology 3, Albert-Ludwigs-Universität Freiburg, Germany
2 Institute for Ageing and Health, Newcastle University, Campus for Ageing and Vitality, UK
3 Centre for Integrated Systems Biology of Ageing and Nutrition, Institute for Ageing and Health, Newcastle University, UK
4 BIOSS Centre for Biological Signalling Studies, Albert-Ludwigs-Universität Freiburg, Germany
5 Center for Systems Biology (ZBSA), Albert-Ludwigs-Universität Freiburg, Germany

Keywords
adenosine monophosphate-dependent kinase; Akt; dynamic network model; insulin; insulin receptor substrate; mammalian target of rapamycin

Correspondence
K. Thedieck, Department of Bioinformatics and Molecular Genetics (Faculty of Biology), Albert-Ludwigs-Universität Freiburg, Schaenzlestr.1, 79104 Freiburg, Germany
Fax: +49 761 203 8352
Tel: +49 761 203 2725
E-mail: kathrin.thedieck@biologie.uni-freiburg.de
Website: http://www.celegans.de/thedieck
D. P. Shanley, Institute for Ageing and Health, Newcastle University, Campus for Ageing and Vitality, Newcastle upon Tyne NE4 5PL, UK
Fax: +44 191 248 1101
Tel: +44 191 248 1105
E-mail: daryl.shanley@ncl.ac.uk
Website: http://www.ncl.ac.uk/iah/staff/profile/daryl.shanley

*These authors contributed equally to this work

(Received 5 January 2012, revised 28 February 2012, accepted 22 March 2012)

doi:10.1111/j.1742-4658.2012.08582.x

Mammalian target of rapamycin (mTOR) kinase responds to growth factors, nutrients and cellular energy status and is a central controller of cellular growth. mTOR exists in two multiprotein complexes that are embedded into a complex signalling network. Adenosine monophosphate-dependent kinase (AMPK) is activated by energy deprivation and shuts off adenosine 5′-triphosphate (ATP)-consuming anabolic processes, in part via the inactivation of mTORC1. Surprisingly, we observed that AMPK not only responds to energy deprivation but can also be activated by insulin, and is further induced in mTORC1-deficient cells. We have recently modelled the mTOR network, covering both mTOR complexes and their insulin and nutrient inputs. In the present study we extended the network by an AMPK module to generate the to date most comprehensive data-driven dynamic AMPK-mTOR network model. In order to define the intersection via which AMPK is activated by the insulin network, we compared simulations for six different hypothetical model structures to our observed AMPK dynamics. Hypotheses ranking suggested that the most probable intersection between insulin and AMPK was the insulin receptor substrate (IRS) and that the effects of canonical IRS downstream cues on AMPK would be mediated via an mTORC1-driven negative-feedback loop. We tested these predictions experimentally in multiple set-ups, where we inhibited or induced players along the insulin–mTORC1 signalling axis and observed AMPK induction or inhibition. We confirmed the identified model and therefore report a novel connection within the insulin–mTOR–AMPK network: we conclude that AMPK is positively regulated by IRS and can be inhibited via the negative-feedback loop.

Abbreviations
AIC, akaike information criterion; AMP, adenosine monophosphate; AMPK, adenosine monophosphate-dependent kinase; ATM, ataxia-telangiectasia mutated; ATP, adenosine 5′-triphosphate; BIC, Bayesian Information Criterion; CaMKK, Ca^{2+}-sensitive calmodulin-dependent protein kinase kinase; CV, coefficient of variance; GAPDH, glyceraldehyde-3-phosphate dehydrogenase; HA-myr-Akt, myristoylated version of Akt; HRP, horseradish peroxidase; IR, insulin receptor; IRE1, inositol-requiring enzyme 1; IRS, insulin receptor substrate; LKB1, liver kinase B1; MOTA, Mean Optimal Transformation Approach; mTOR, mammalian target of rapamycin; mTORC1, mammalian target of rapamycin complex 1; mTORC2, mammalian target of rapamycin complex 2; NFL, negative-feedback loop; PDK1, phosphoinositide-dependent protein kinase 1; p.i., postinduction; PI3K, phosphatidylinositol 3-kinase; PRAS40, proline-rich Akt substrate of 40 kDa; PTEN, phosphatase and tensin homologue; p70-S6K, S6-kinase; shRaptor, inducible short hairpin Raptor knockdown;TAK1/MAP3K7, transforming growth factor-beta-activated kinase-1; TSC1–TSC2, tuberous sclerosis complex 1/2 dimer; 4E-BP, 4E-binding protein.

Introduction

Mammalian target of rapamycin (mTOR) kinase is a central controller of cellular growth and metabolism and is conserved in all eukaryotes. mTOR controls anabolic and catabolic processes, including translation, ribosome biogenesis and autophagy, in response to nutrients (amino acids), energy and growth factors (insulin). mTOR exists in two multiprotein complexes – mTOR complex 1 (mTORC1) and mTOR complex 2 (mTORC2) – which are functionally and structurally distinct: mTORC1 contains Raptor and proline-rich Akt substrate of 40 kDa (PRAS40) as specific binding partners and controls cellular growth, whereas mTORC2 comprises mammalian stress–activated protein kinase–interacting protein 1 (mSIN1), proline rich protein 5 (PRR5)/PRR5-Like (PRR5L) and Rictor, and controls apoptosis as well as spatial growth via the actin cytoskeleton [1,2].

Being a central growth regulator, mTOR is tightly embedded into a complex signalling network, transducing insulin signals via the insulin receptor (IR), the insulin receptor substrate (IRS), class I phosphatidylinositol 3-kinases (PI3Ks), phosphoinositide-dependent protein kinase 1 (PDK1) and the protein kinase A/protein kinase G/protein kinase C-family (AGC) kinase, Akt (also known as PKB). Akt inhibits the tuberous sclerosis complex 1/2 dimer (TSC1–TSC2), which is the inhibitory GTPase-activating protein for Rheb [1–4]. Via this cascade, Akt induces mTORC1. mTORC1 phosphorylates S6-kinase (p70-S6K), the translation initiation regulator 4E-binding protein (4E-BP) and the mTORC1-inhibitor PRAS40 [5–12]. Whereas PRAS40 inhibits mTORC1 activity, p70-S6K and 4E-BP mediate mTORC1 downstream effects. Furthermore, active p70-S6K phosphorylates and inhibits the IRS, which consequently cannot activate PI3K in response to insulin. This mechanism results in a negative-feedback loop (NFL), which inhibits upstream insulin signalling upon mTORC1 activation [2]. We have recently modelled this network and shown that whereas mTORC1 is induced via the above described signalling cascade, the induction of mTORC2 occurs via a distinct PI3K that is insensitive to the NFL [13].

mTOR not only responds to the insulin network but is also connected to many other signalling cascades, including adenosine monophosphate (AMP)-dependent kinase (AMPK), Wnt signalling and the mitogen-activated protein kinase kinase kinase (MEK)/extracellular signal-regulated kinase (Erk) pathway. To incorporate further kinase inputs into our dynamic network model, we decided to focus on the development of an AMPK module. AMPK turns on catabolic adenosine 5′-triphosphate (ATP)-generating pathways and shuts off ATP-consuming anabolic processes, such as ribosome biogenesis and translation, in part via the inactivation of mTORC1 [14]. AMPK is activated by both energy deprivation and by the liver kinase B1 (LKB1) (or STK11). Inhibition of glycolytic flux leads to a high AMP/ATP ratio, activating AMPK by direct, allosteric AMP binding. LKB1 activates AMPK by phosphorylating AMPK-T172 and thereby negatively regulates mTORC1 [14]. Although LKB1 seems to be the main upstream kinase of AMPK, LKB1 also phosphorylates 12 other kinases [15], termed AMPK-related kinases. The physiological functions of these kinases are still poorly understood. Apart from LKB1, several other kinases can phosphorylate AMPK-T172 independently of the cellular energy status, including Ca^{2+}-sensitive calmodulin-dependent protein kinase kinase (CaMKK) [16–19] and transforming growth factor-beta-activated kinase-1 (TAK1/MAP3K7) [20–22]. Also, ataxia-telangiectasia mutated (ATM) kinase-dependent [23,24] or inositol-requiring enzyme 1 (IRE1)-dependent [25] induction of AMPK have been reported.

To inhibit mTORC1 signalling, AMPK multiply phosphorylates and activates TSC2 when cellular energy is low [26]. In addition, AMPK also directly phosphorylates the essential mTORC1 component Raptor on two serine residues [27]. This phosphorylation induces 14-3-3 to bind to Raptor and is required for mTORC1 inhibition by energy deprivation.

We observed, in the present work, that AMPK not only responds to energy deprivation but is also strongly activated by insulin and is further induced in Raptor-deficient cells. These findings are in line with others [23,28,29]; however, the underlying signalling events have been only poorly investigated to date. In order to define the intersection via which AMPK is activated by the insulin network, we generated a data-driven dynamic AMPK–mTOR network model and used a combined modelling-experimental approach. We compared simulations for different model structures with our observed AMPK dynamics. Hypotheses ranking suggested that the most probable intersection between insulin and AMPK was the IRS, and that the effects of canonical IRS downstream cues on AMPK are mediated via the NFL. We tested and confirmed these predictions experimentally in multiple set-ups. We report here a novel connection within the insulin–mTOR–AMPK network: we conclude that AMPK is positively regulated by IRS and can be inhibited via the NFL.

Results

An insulin–TOR–AMPK model

We recently described the development of a dynamic mTOR network model [13] that covered insulin and amino-acid signalling as mTORC1 regulators. AMPK is another important mTOR regulator that suppresses mTORC1 activity in response to energy deprivation [14] and we decided to add this regulation to our model. We introduced the following novel connection into the existing network structure [13]: AMPK phosphorylation at T172 allows AMPK to phosphorylate the species TSC1_TSC2 at S1387, which leads to the activation of TSC1–TSC2 and the subsequent inhibition of mTORC1. Conversely, the phosphorylation of the species TSC1_TSC2 at T1462 by Akt_pT308 inhibits the TSC1_TSC2 complex, activating mTORC1. Finally, the species Akt_pS473, PRAS40_pT246 and PRAS40_pS183 were defined as supplementary readouts for mTORC2, Akt and mTORC1, respectively.

In order to calibrate the AMPK module and connect it to our existing mTOR model, we acquired AMPK time courses under the same conditions that we had used for calibration of the dynamic mTOR network model [13]. These were starvation of serum and amino acids followed by network induction by insulin and amino acids. AMPK is described to be induced in Raptor-deficient cells [28,29]. Therefore, we also investigated AMPK activity upon gradual knockdown in an inducible short hairpin Raptor knockdown (shRaptor) HeLa cell line. The knockdown was induced by doxycycline treatment for 3, 2 or 0 days. Cells were starved for 16 h and activated with insulin and amino acids from 3 min up to 100 min postinduction (p.i.) (Fig. 1A). As previously described [13], the direct mTORC1 substrate, p70-S6K-pT389, was activated from 20 min onwards and displayed reduced phosphorylation upon induction of Raptor knockdown. AMPK activity was monitored by detecting phosphorylation at T172, reflecting active AMPK [14]. Although AMPK is known to be induced by energy depletion [14], we found, to our surprise, that AMPK-pT172 is also strongly induced by insulin and amino acids, and induction was apparent at only 3 min p.i. Overall, AMPK-pT172 induction decreased with time. As expected, AMPK-pT172 was more strongly induced upon Raptor knockdown, and this was observable from 20 min p.i. onwards (Fig. 1A). Upon activation, AMPK phosphorylates TSC2 at S1387, leading to TSC2 activation and subsequent inhibition of mTORC1 [26,30]. Therefore, we used TSC2-S1387 as a

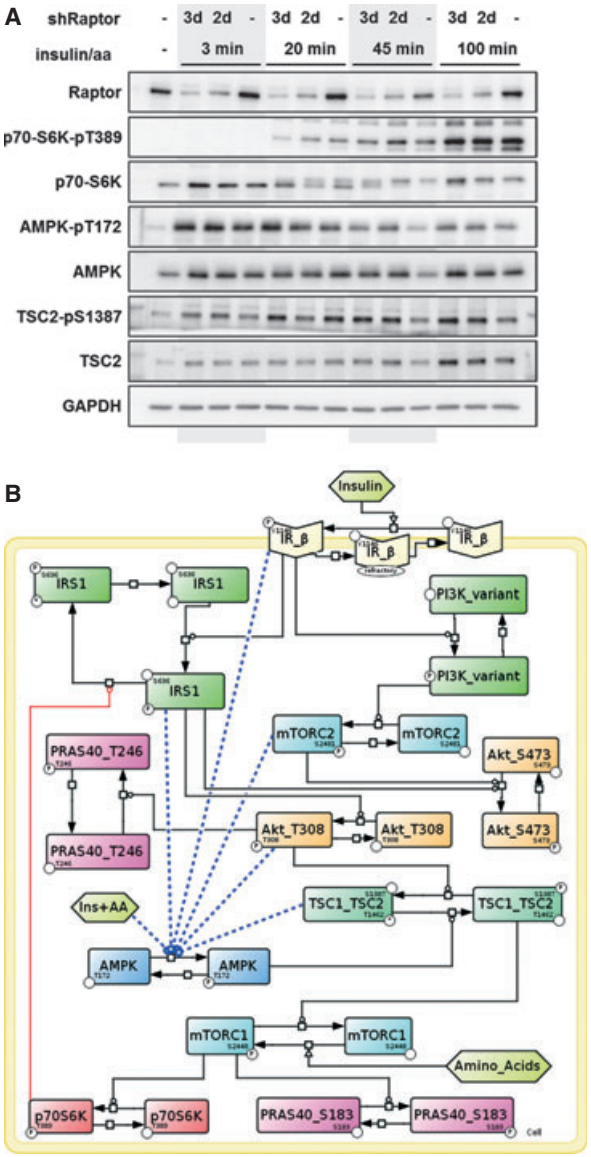

Fig. 1. Set up of an AMPK module. (A) AMPK is induced upon insulin induction. A gradual Raptor knockdown was induced in HeLa cells by doxycyline treatment for the indicated times. Cells were serum/amino acid starved for 16 h and restimulated with amino acids and 100 nM insulin for 3, 20, 45 or 100 min. (B) Insulin–mTOR–AMPK model. This model integrates our previous insulin–mTOR model with AMPK regulation. Six hypotheses of AMPK activation are investigated (blue dotted lines). Except for the insulin- and IR-beta (IR-β)-induced AMPK hypotheses, all others implicitly assume AMPK as being dependent on the p70-S6K NFL. aa or AA, amino acids; Ins, insulin.

second AMPK readout, to confirm our findings on AMPK activation. Indeed, TSC2-pS1387 followed AMPK-pT172 with some delay, starting 20 min p.i. and was induced by insulin and amino acids, and in Raptor knockdown cells. All signal intensities were

quantified, and descriptive statistics were computed over three replicates. The experimental mean time courses were used to calibrate the model parameters.

Although it has been described previously that AMPK is induced by insulin-like growth factor 1 (IGF-1) [23], this signalling connection has been only poorly explored to date. Therefore, in the present study we systematically investigated possible AMPK activators along the insulin–mTORC1 axis. mTORC1 is maximally induced at 30-45 min p.i. [13]. As AMPK induction by insulin peaked as early as 3 min p.i., and AMPK was induced by Raptor knockdown (i.e. mTORC1 inhibition), we selected, as candidate AMPK activators, the species upstream of mTORC1:

1. Insulin, where insulin is considered as constant and direct input to AMPK;
2. IR_beta_pY1146, reflecting IR activation;
3. IRS1_p, reflecting IRS1 activation by the IR;
4. mTORC2_pS2481, reflecting mTORC2 activation by insulin and amino acids [13];
5. Akt_pT308, reflecting Akt activation downstream of PI3K; and
6. TSC1_TSC2_pT1462, reflecting TSC1–TSC2 deactivation by Akt.

A graphical representation of our insulin–mTOR–AMPK model, depicting our six alternative hypotheses of AMPK activation, is provided in Fig. 1B.

Parameter estimation and identifiability

A specific model was instantiated for each hypothesis and calibrated using the same data sets and the Matlab Toolbox PottersWheel [31]. Before calibrating the models, structural identifiability analysis was performed using the software GenSSI [32]. This software calculated the symbolic solution of the problem, computing Lie derivatives for each hypothesis and confirming structural global identifiability for all six models. For the IRS1-induced AMPK model, structural identifiability analysis is reported in Fig. 2A, showing that all the parameters were structurally identified in the first-order (blue circles) or second-order (magenta circles) identifiability tableau.

To calibrate the models, experimental time courses upon insulin/amino acid induction for nine readouts (IR_beta_pY1146, IRS1_pS636, Akt_pT308, Akt_pS473, mTORC1_pS2448, mTORC2_pS2481, p70S6K_pT389, PRAS40_pT246 and PRAS40_pS183; data set 1) in wild-type cells along the insulin–mTOR signalling axis were used in combination with time courses under gradual mTORC1 inhibition (Raptor knockdown; data set 1) in wild-type cells, as measured previously [13]. Furthermore, in order to calibrate the species AMPK_pT172 and TSC1_TSC2_pS1387, the five time points (0, 3, 20, 45 and 100 min p.i.; Fig. 1A) without knockdown induction (i.e. corresponding to wild type), were added as an additional data set (data set 3).

Parameter estimation was executed for each model independently over multiple data sets in order to reduce the bias of the solution and therefore overfitting. However, the addition of data sets used to calibrate a model can lead to a serious increment of variance, particularly because of the increase in intrinsic noise in experimental data, which does not permit to estimate the parameters of the model correctly. Our second data set was characterized by three different levels of Raptor knockdown, obtained by doxycycline treatment for 0, 2 or 3 days, respectively (subsets 1-3). We found a satisfactory bias–variance trade-off by combinatorially and singularly testing these three subsets and eventually selecting only the subset of Raptor knockdown induced by doxycycline treatment for 3 days (subset 3). Subset 3 was selected as it represented the strongest signal reduction and consequently novel information with respect to wild-type time courses (data set 1) for calibrating the model. Moreover, the readouts in our data sets (data set 1, data set 2-subset 3, data set 3) were scaled in order to obtain species time courses of similar intensity. This distributes the cost of the solution equally over the simulated time courses, approximating the data and avoiding an implicit preference ranking of calibration.

For calibrating the models, we only estimated the kinetic rate-constant parameters, whereas the species protein concentrations were determined from our immunoblot time courses by selecting the corresponding readout maximum intensity plus two standard deviations measured at that time point. The addition of two standard deviations to the maximum signal peak guaranteed the avoidance of species protein-saturation conditions. The kinetic rate constants regulating PI3K-variant dynamics were fixed *a priori* assuming a time course similar to the insulin receptor. In fact, no experimental data are available for this PI3K insensitive to the NFL and it is more likely that it follows the IR-beta receptor than other curves. Furthermore, fixing these parameters led us to a full structural identifiability of the model.

A posterior identifiability analysis was performed using the Mean Optimal Transformation Approach (MOTA) plugin [31,33] after selecting the 50% of the best fits (shown in Fig. 2B for the IRS1-induced AMPK model). This analysis revealed that high parameter correlations had a coefficient of variation (CV) lower than 0.05 for all our models except for the

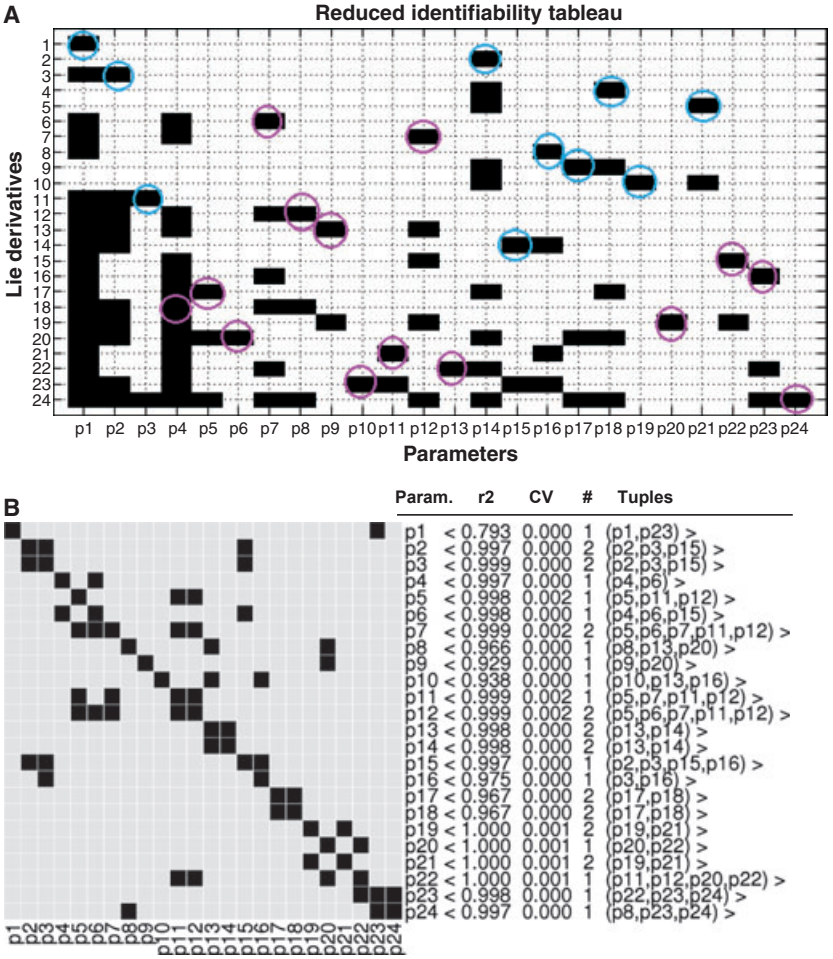

Fig. 2. Identifiability analysis for the IRS1-induced AMPK model (hypothesis 3). (A) Structural identifiability analysis was performed using the software GenSSI *a priori*. In the reduced identifiability tableau, blue circles indicate the parameters detected directly as structurally globally identifiable at the first-order tableau, whereas magenta circles highlight the parameters detected as structurally globally identifiable at the second-order tableau after computing the symbolic solution. (B) MOTA identifiability analysis was executed using the 50% of the best fits of the calibration fits sequence. A correlation among a set of parameters is indicated by the tuple of correlated parameters, their correlation coefficient (r2), the CV and the number of times that this correlation was identified by varying the parameters of the tuple (#). Even though high correlations were found among some parameters, the corresponding CV was lower than 0.002, which can be explained as a numeric approximation error in the fit sequence calibration process. (*) $r^2 > 0.9$ and CV > 0.1 (**) $r^2 > 0.9$ and CV > 0.1 and #>1. Param., parameter.

IR-beta-induced AMPK model (hypothesis 2; Fig. S1). For this model, MOTA analysis highlighted high correlation and a high CV for the pair of parameters regulating AMPK dynamics. Model identifiability was obtained after fixing one of the two parameters and recalibrating the other in a second round of calibration. In combination with the previous analysis, we also checked parameter nonidentifiability by directly

analysing the estimated percentage of standard deviations of the parameters, computed over the 50% best fits, and considering nonidentifiable the parameters with a standard deviation percentage higher than a threshold of 5%. Table 1 presents the values for the estimated parameters, with mean, standard deviation and CV values for the IRS1-induced AMPK model showing parameter identifiability. Sensitivity analysis for the same model is provided in Fig. S2, showing a balanced sensitivity among the parameters and that all were required.

In summary, we independently calibrated six models sharing the main network structure and differing in AMPK activation. We were therefore able to investigate our central question, of finding at which level in the network AMPK is induced by insulin.

Intersection level of the signalling from insulin to AMPK: model simulation analyses over AMPK-pT172 and TSC2-pS1387 readouts

Once the parameter estimation was achieved, the simulated time courses for the readouts AMPK_pT172 and TSC1_TSC2_pS1387 of each model were compared with the corresponding experimental time courses (see Fig. 3). Surprisingly, we observed that the readouts AMPK_pT172 and TSC1_TSC2_pS1387 for the IRS1-induced AMPK model (hypothesis 3) fitted the data with high accuracy, whereas the goodness-of-fit decreased for species downstream of IRS1 (Akt and TSC1-TSC2; hypotheses 5 and 6) and upstream of IRS1 (insulin, IR-beta; hypotheses 1 and 2), as indicated by the measure χ^2. Furthermore, the two readouts showed a poorer fit for the mTORC2-induced AMPK model (hypothesis 4). At this point, we questioned whether these local differences could lead to a possible ranking of the overall models. In order to achieve this, several additional likelihood-based statistical criteria, such as the Akaike Information Criterion [34] [AIC, Akaike Information Criterion corrected (AICc)] and the Bayesian Information Criterion [35] (BIC), were used besides the total χ^2, to estimate the goodness-of-fit calculated over the entire models. These estimations allowed us to establish a ranking of the hypotheses in accordance with the goodness-of-fit (Table 2). All values obtained were consistent between these measures and with the above observations in selecting the IRS1-induced AMPK model (hypothesis 3) as the most probable model. The remaining simulated versus experimental time courses for the IRS1-induced AMPK model are reported in Fig. S3. A Systems Biology Markup Language (SBML) model is provided for the IRS1-induced AMPK hypothesis.

In summary, hypotheses ranking suggested that IRS (hypothesis 3) was the most probable inducer of AMPK in response to insulin. This, in turn, suggested that downstream cues of IRS1 could affect AMPK via the NFL, which would be in line with the observed induction of AMPK in mTORC1-deficient cells (Fig. 1A, [28,29]). We then tested this experimentally.

Experimental testing: AMPK activation is IRS dependent and indirectly regulated via the NFL

Hypothesis 3 predicts that IRS will be required for AMPK induction by insulin. We therefore tested first whether IRS hyperactivation alone would result in increased AMPK-T172 phosphorylation. To achieve this we overexpressed wild-type IRS-1 (Myc-IRS-1 WT) or mutagenized IRS-1 variants, resembling either IRS-1 constitutively phosphorylated by S6K (Myc-IRS-1 S636/639 D) or constitutively unphosphorylated on the same sites (Myc-IRS-1 S636/639 A) [36]. The variants are NFL insensitive and whereas the D variant is less active, the A variant will be hyperactive. The constructs were overexpressed in HeLa cells (Fig. 4A). As expected, Myc-IRS-1 WT and Myc-IRS-1 S636/639 A strongly induced Akt-pT308 and mTORC1 activity towards p70-S6K-T389, whereas Myc-IRS-1 S636/639 D did not. Importantly, AMPK-pT172 was induced moderately by Myc-IRS-1 WT and strongly by Myc-IRS-1 S636/639 A, but was refractory to overexpression of Myc-IRS-1 S636/639 D. This finding is in line with hypothesis 3, which suggests the requirement of active IRS for AMPK induction by insulin. To further confirm our finding we also analysed the AMPK target site, TSC2-S1387, upon overexpression of Myc-IRS-1 WT (Fig. 4B). TSC2-pS1387 was strongly induced, again suggesting positive regulation of AMPK by IRS-1.

IRS-1 hyperactivation will strongly induce PI3K activity [36], and we did not differentiate, in our hypothesis 3, between IRS and PI3K activity. We therefore next tested whether PI3K also positively affects AMPK. We inhibited PI3K with wortmannin before induction with insulin/amino acids (Fig. 4C): as expected, wortmannin inhibited Akt-pT308, downstream of PI3K. In contrast, wortmannin induced AMPK-T172 phosphorylation. To confirm this finding in a complementary set-up, we overexpressed the PI3K antagonist phosphatase and tensin homolog (PTEN): PI3K generates phosphatidylinositol (3,4,5)-trisphosphate (PIP3), leading to the induction of PDK1, Akt and their downstream targets; however, PTEN dephosphorylates PIP3, thereby counteracting PI3K activity. As expected, PTEN overexpression strongly

Table 1. Parameter table for the IRS1-induced AMPK model (hypothesis 3). The estimated kinetic rate constants, together with the species concentrations, are provided. The mean, SD and per cent of the SD over the mean, computed over the 50% best fits, are also indicated. These statistics shows that all 24 estimated parameters could be fixed at the first round of calibration. Scaling factor parameters and observable variables are also indicated. The SBML model given in Model S2 (Supporting information) is configured with these parameter values.

Parameter name (AMPK induced by the IRS1 model) [kinetic rate constants (min^{-1})]	Calibration [mean ± SD (%)]	Value
p1 = IR_beta_phosphorylation_by_Insulin	0.124278 ± 1.21324e-05 (0%)	0.124273
p2 = IR_beta_pY1146_dephosphorylation	0.396251 ± 3.02338e-05 (0%)	0.396235
p3 = IR_beta_ready	0.0532808 ± 6.9999e-06 (0%)	0.053277
p4 = IRS1_phosphorylation_by_IR_beta_pY1146	0.00491628 ± 5.46924e-07 (0%)	0.00491599
p5 = IRS1_p_phosphorylation_by_p70S6K_pT389	1681.94 ± 3.80623 (0%)	1682.75
p6 = IRS1_pS636_dephosphorylation	0.0130526 ± 4.45303e-06 (0%)	0.01305
p7 = AMPK_T172_phosphorylation	9.79357 ± 0.0177607 (0%)	9.79766
p8 = AMPK_pT172_dephosphorylation	0.0107217 ± 4.13895e-07 (0%)	0.0107215
p9 = Akt_pT308_dephosphorylation	0.00335553 ± 3.70977e-07 (0%)	0.00335545
p10 = Akt_pS473_dephosphorylation	0.00640225 ± 1.80374e-07 (0%)	0.00640216
p11 = Akt_S473_phosphorylation_by_mTORC2_pS2481_n_IRS1_p	13.1374 ± 0.0302136 (0%)	13.1442
p12 = Akt_T308_phosphorylation_by_IRS1_p	6.9152 ± 0.0123683 (0%)	6.91811
p13 = mTORC1_pS2448_dephosphorylation_by_TSC1_TSC2_pS1387	0.0106657 ± 9.77042e-07 (0%)	0.0106652
p14 = mTORC1_S2448_activation_by_Amino_Acids	0.00438932 ± 3.03977e-07 (0%)	0.00438916
p15 = mTORC2_pS2481_dephosphorylation	0.0183743 ± 1.62188e-06 (0%)	0.0183735
p16 = mTORC2_S2481_phosphorylation_by_PI3K_variant_p	0.375358 ± 1.34923e-05 (0%)	0.375353
p17 = p70S6K_pT389_dephosphorylation	0.0113508 ± 6.03276e-07 (0%)	0.0113512
p18 = p70S6K_T389_phosphorylation_by_mTORC1_pS2448	0.0018404 ± 3.38908e-08 (0%)	0.00184043
p19 = PRAS40_pS183_dephosphorylation	2.33046 ± 0.00198802 (0%)	2.33014
p20 = PRAS40_pT246_dephosphorylation	1.60545 ± 0.00132301 (0%)	1.60513
p21 = PRAS40_S183_phosphorylation_by_mTORC1_pS2448	0.187646 ± 0.000157968 (0%)	0.187621
p22 = PRAS40_T246_phosphorylation_by_Akt_pT308	0.137756 ± 0.000112104 (0%)	0.137729
p23 = TSC1_TSC2_S1387_phosphorylation_by_AMPK_pT172	0.0365597 ± 4.61345e-06 (0%)	0.0365589
p24 = TSC1_TSC2_T1462_phosphorylation_by_Akt_pT308	0.0177568 ± 1.993e-06 (0%)	0.0177562
p25 = PI3K_variant_p_dephosphorylation	Assumed	10
p26 = PI3K_variant_phosphorylation_by_IR_beta_pY1146	Assumed	0.01
Concentrations (AU)		
u1 = Insulin (INPUT)	Fixed	10
u2 = Amino_Acids (INPUT)	Fixed	10
x1 = IR_beta	Determined	16.56070782
x4 = IRS1	Determined	18.93446968
x7 = AMPK	Determined	20.50644836
x9 = Akt_T308	Determined	21.41085271
x11 = Akt_S473	Determined	12.25170805
x13 = mTORC1	Determined	25.14
x15 = mTORC2	Determined	18.79587754
x17 = p70S6K	Determined	14.30096315
x19 = PRAS40_S183	Determined	13.56128255
x21 = PRAS40_T246	Determined	17.55000883
x23 = TSC1_TSC2_pT1462	Determined	14.9175
x25 = PI3K_variant	Determined	18.93446968
x2 = IR_beta_pY1146; x3 = IR_beta_refractory; x5 = IRS1_p; x6 = IRS1_pS636; x8 = AMPK_pT172; x10 = Akt_pT308; x12 = Akt_pS473; x14 = mTORC1_pS2448; x16 = mTORC2_pS2481; x18 = p70S6K_pT389; x20 = PRAS40_pS183; x22 = PRAS40_pT246; x24 = TSC1_TSC2_pS1387; x26 = PI3K_variant_p	Fixed	0
Scaling factors		
s1 = scale_IR_beta_pY1146_obs; s2 = scale_IRS1_pS636_obs; s3 = scale_AMPK_pT172_obs; s4 = scale_Akt_pT308_obs; s5 = scale_Akt_pS473_obs; s6 = scale_TSC1_TSC2_pS1387_obs; s7 = scale_mTOR_pS2448_obs; s8 = scale_mTOR_pS2481_obs; s9 = scale_p70S6K_pT389_obs; s10 = scale_PRAS40_pT246_obs; s11 = scale_PRAS40_pS183_obs	Fixed	1

Table 1. (Continued).

Parameter name (AMPK induced by the IRS1 model) [kinetic rate constants (min^{-1})]	Calibration [mean ± SD (%)]	Value
Observables (AU)		
y1 = IR_beta_pY1146_obs	Assigned	s1*x2
y2 = IRS1_pS636_obs	Assigned	s2*x6
y3 = AMPK_pT172_obs	Assigned	s3*x8
y4 = Akt_pT308_obs	Assigned	s4*x10
y5 = Akt_pS473_obs	Assigned	s5*x12
y6 = TSC1_TSC2_pS1387_obs	Assigned	s6*x14
y7 = mTOR_pS2448_obs	Assigned	s7*x16
y8 = mTOR_pS2481_obs	Assigned	s8*x18
y9 = p70S6K_pT389_obs	Assigned	s9*x20
y10 = PRAS40_pT246_obs	Assigned	s10*x22
y11 = PRAS40_pS183_obs	Assigned	s11*x24
Compartments (AU)		
c1 = Cell	Fixed	1

inhibited mTORC1 activity towards p70-S6K-T389 (Fig. 4D). In agreement with our findings for wortmannin, increased PTEN levels activated AMPK, as evidenced by AMPK-pT172 induction. We conclude that AMPK is induced by IRS, but inhibited by PI3K. The induction of AMPK in response to PI3K inhibition is in line with our own and previous findings on AMPK induction in mTORC1-deficient cells and might be mediated via the NFL. In other words, if IRS is required for AMPK induction, inhibition of the NFL (targeting IRS) should induce AMPK.

If this reasoning and our hypothesis 3 hold true, activation of Akt and subsequent hyperactivation of the NFL should inhibit AMPK. We tested this prediction by overexpressing a myristoylated version of Akt (HA-myr-Akt) [37], which is constitutively localized to the plasma membrane and does not require IRS or PI3K for its activation. As expected for Akt hyperactivation, expression of HA-myr-Akt strongly induced the Akt target site TSC2-pT1462 (Fig. 4E). TSC2-T1462 phosphorylation leads to inhibition of the TSC1-TSC2 complex and hyperactivates mTORC1. Also, mTORC1 activity towards p70-S6K-T389 was expectedly strongly induced by HA-myr-Akt overexpression, and p70-S6K activation induces the NFL. In contrast, AMPK-pT172 was inhibited by HA-myr-Akt and the same could be confirmed for the AMPK target site, TSC2-S1387, which is required for TSC1-TSC2 activation. This result is in agreement with our model 3, predicting a negative effect of Akt on AMPK, via the NFL and IRS. These data also directly exclude hypotheses 5 and 6, which are on ranks 2 and 3 in our hypotheses ranking (Table 2).

In summary, we chose here four independent experimental set-ups to test the predictions of model 3, which was ranked 1 in our hypothesis ranking. All experiments provide strong evidence for model 3, where IRS induces AMPK and exclude the other hypotheses where other insulin downstream cues mediate AMPK activation: we show that IRS-1 strongly induces AMPK, whereas the PI3K-Akt-mTORC1 signalling axis suppresses AMPK (Fig. 5A). This is in line with the NFL (downstream of PI3K, Akt and mTORC1) suppressing AMPK, which is predicted by our model 3. The network structure of our final model is depicted in Fig. 5B.

What are the biological implications of our findings? We and others show that in HeLa cells AMPK is induced by insulin and amino acids (Fig. 1A, [23]). However, HeLa cells are particular in the sense that they do not express the AMPK upstream kinase, LKB1 [23,24]. Therefore, it was important to address whether the induction of AMPK by insulin and amino acids, observed here, is a general feature of AMPK signalling, or whether it remains restricted to LKB1-deficient cells. Hence, we tested the effect of insulin and amino acid induction on AMPK activity in C2C12 myocytes, which are LKB1 positive (Fig. 4F). We observed AMPK induction by insulin and amino acids also in C2C12 cells, underlining the general importance of our findings.

Discussion

In the present study we observed induction of AMPK by insulin and amino acids. Although this has been reported previously [23], ours is the first study to explore systematically the underlying signalling interconnections within the insulin–mTOR network. To achieve this we systematically postulated

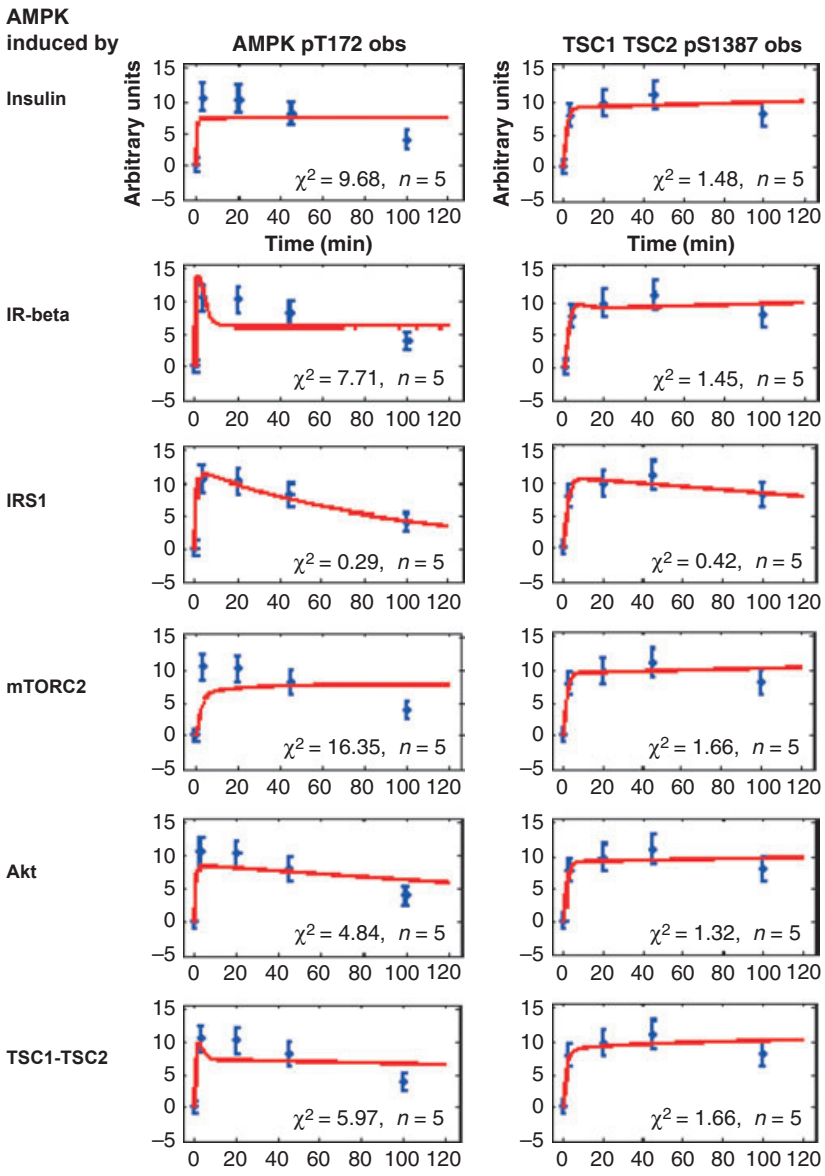

Fig. 3. Prediction: intersection of insulin and AMPK signalling at the level of IRS1. Simulated time courses (red lines) versus experimental data (blue points) for AMPK–pT172 and TSC1–TSC2–pS1387 (columns) for the six hypotheses: insulin-induced AMPK, IR-beta-induced AMPK, IRS-induced AMPK, mTORC2-induced AMPK, Akt-induced AMPK and TSC1–TSC2-induced AMPK (rows). These predictions suggest that AMPK could be regulated by kinases downstream of the IR. The IRS-induced AMPK model showed the best fit to our experimental data. Experimental data error bars indicate the SEM calculated over three repetitions. The SBML model given in Model S2 (Supporting information) reproduces the AMPK induction by IRS1. obs, observable.

Table 2. Statistical ranking of the models. N. Points = 130; K. Parameters = 24. The quality of fitting measures were used to determine a ranking of the investigated models. The IRS1-induced AMPK model showed the lowest χ^2 value, indicating that this model was the most probable (values in bold). AIC, AICc and BIC values are reported as additional measures.

Hypothesis no.	AMPK induction by	χ^2	*P*-value (*M*)	*P*-value ($N - p$)	AIC	AICc	BIC	Rank
1	Insulin	80.3086	0.999809	0.970256	367.233	378.66	436.053	5
2	IR-beta	78.1345	0.999908	0.980596	365.058	376.487	433.879	4
3	IRS1	**68.0217**	**0.999999**	**0.998462**	**354.946**	**366.374**	**423.767**	1
4	mTORC2	90.1238	0.99694	0.865145	377.048	388.476	445.869	6
5	Akt	75.5272	0.999964	0.988951	362.451	373.88	431.272	2
6	TSC1–TSC2	76.4666	0.99995	0.986376	363.391	374.819	432.211	3.

molecules along the insulin–mTORC1 signalling axis as putative AMPK activators. Furthermore, we presumed that the putative AMPK inducer would be upstream of mTORC1, first, because AMPK was induced earlier (3 min p.i.) than mTORC1 and its downstream targets and, second, because Raptor

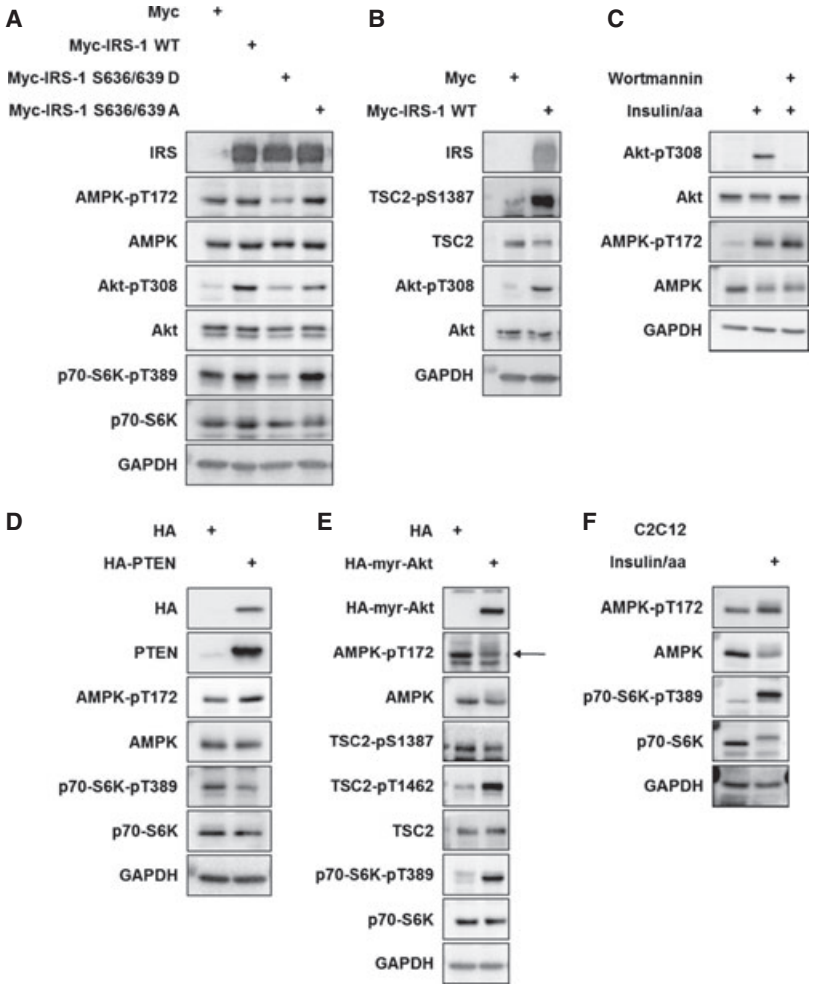

Fig. 4. Experimental testing: IRS induces AMPK. (A) IRS overexpression induces AMPK. HeLa cells were harvested 24 h after transfection with the indicated IRS-1 constructs. The mutagenized Myc-IRS-1 S6367/639 D construct mimics the constitutive phosphorylation by S6K, whereas Myc-IRS-1 S6367/639 A resembles constitutively unphosphorylated IRS and cannot be inhibited by S6K and the NFL. (B) IRS overexpression induces TSC2 phosphorylation by AMPK. HeLa cells were harvested 24 h after transfection with Myc-IRS-1 WT. (C) The PI3K inhibitor wortmannin induces AMPK. HeLa cells were starved and treated with 100 nM wortmannin or carrier before restimulation with insulin/amino acids. (D) Overexpression of the PI3K antagonist, PTEN, induces AMPK. HeLa cells were transfected 24 h before harvesting. Cells were starved of serum/amino acids before restimulation with insulin/amino acids. (E) Constitutively active Akt inhibits AMPK. HeLa cells were harvested 24 h after transfection with myristoylated Akt (HA-myr-Akt). (F) Insulin/amino acids induce AMPK in LKB1-positive C2C12 myocytes. aa, amino acids; WT, wild type.

inhibition induced AMPK (Fig. 1A). Applying a hypothesis ranking approach, we successfully used a dynamic insulin–mTOR–AMPK model for hypothesis prioritization.

In accordance with our hypothesis that best fits the data (hypothesis 3), we confirmed experimentally that IRS activates AMPK. In contrast, all tested IRS downstream cues within the PI3K–mTORC1 axis (PI3K, Akt, mTORC1) inhibited AMPK. This is in line with our prioritized model where the NFL – downstream of mTORC1 and S6K – inactivates IRS for PI3K activation as well as for AMPK induction. AMPK was induced by wild-type IRS and a mutagenized IRS version that cannot be targeted by the NFL, whereas AMPK was refractory to expression of an IRS version that resembles constitutively NFL-targeted IRS (Fig. 4A). Also this finding strongly suggests that indeed the NFL might inactivate IRS, not only for PI3K but also for AMPK induction.

From a modelling point of view, a comprehensive mTOR network has been studied statically, [38] and parts of the mTOR network have been modelled dynamically [13,39–45]. The network presented in this study is

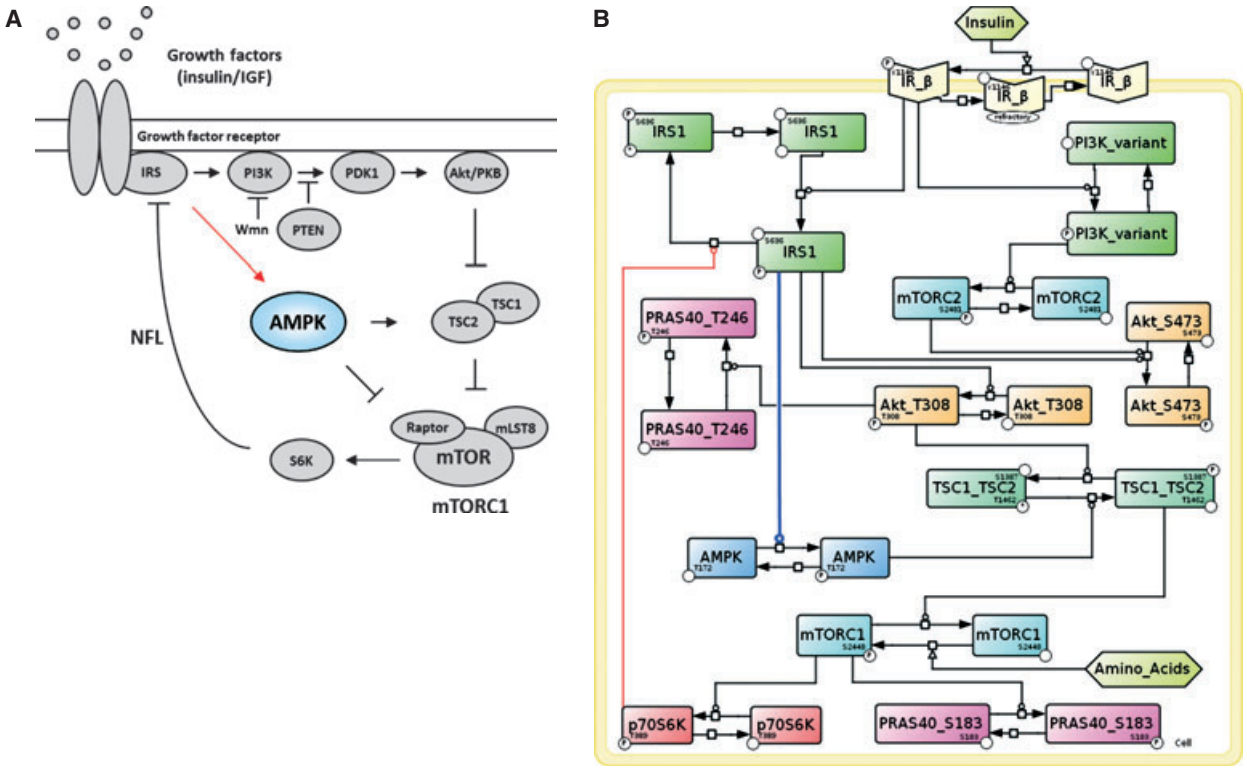

Fig. 5. New model structure: IRS is required for AMPK induction by insulin. (A) Schematic representation of the insulin-induced mTORC1 pathway, including IRS-dependent AMPK induction. Importantly, the NFL via IRS targets not only PI3K but also AMPK. Wmn, wortmannin. (B) Insulin–mTOR–AMPK model describing IRS as a regulator of AMPK.

the most extensive mTOR–AMPK model of which we are aware. Six models were defined and calibrated using our experimental data. The models shared the main network structure, but differed for the AMPK activation mechanism. After repeating cycles of parameter calibration and identifiability for each model, likelihood-based statistical measures were used to estimate a model ranking, based on the goodness-of-fit between each model and the experimental data.

In the present study we observed transient induction of AMPK by insulin and identified active IRS as an AMPK inducer. On the other hand, AMPK inhibits IRS by phosphorylation of IRS-1-S794 [46–48]. Could this mechanism be connected to the AMPK induction by IRS observed here? It is conceivable that two antagonistic mechanisms are mediated by IRS: when IRS is active, it will activate AMPK – and at the same time AMPK could directly, via IRS, contribute to the inhibition of insulin signalling. This putative mechanism clearly deserves further mechanistic investigation.

It is important to note that HeLa cells, which were used in the present study, do not express LKB1. This suggests that AMPK induction by insulin and IRS is LKB1 independent, at least in HeLa cells. Which other kinase could be responsible? AMPK phosphorylation in HeLa (and other) cells is mediated by the kinase ATM [23,24]. Interestingly, AMPK induction by ATM occurs in a tyrosine-kinase dependent, but PI3K-independent, manner [24]. This is consistent with our finding that IRS, but not PI3K, induces AMPK (Fig. 4A–D). Other possible candidates for LKB1-independent AMPK induction are the kinases CaMKK [16–19], TAK1 [20–22] or IRE1 [25].

What is the relevance of the mechanism reported here in LKB1-expressing cells? First, Suzuki *et al.* [23] reported the IGF-1 inducibility of AMPK, not only in LKB1-deficient HeLa cells, but also in LKB1-expressing PANC1 cells. Also, our own data confirm the inducibility of AMPK by insulin and amino acids in LKB1-expressing C2C12 myocytes (Fig. 4F), suggesting that this mechanism may be present in a larger number of cell types. Furthermore, at least two other studies have reported that AMPK is induced by mTORC1 [28] or S6K [29] ablation in mice. This suggests that IRS-dependent AMPK induction might become particularly prominent under conditions when the NFL is inhibited. Hence, IRS-dependent AMPK induction may exert some of the beneficial effects that

have been observed for mTOR-inhibitor treatment of metabolic and tumour diseases [49].

What could be the biological function of a transient induction of AMPK by insulin? First, AMPK inhibits mTORC1 signalling at two levels: TSC1–TSC2 and mTORC1 itself. Therefore, this transient AMPK induction in response to insulin might – in addition to the NFL – serve as a second mechanism to prevent mTORC1 hyperactivation. As an additional benefit, AMPK activation might serve as a protective mechanism to cellular stress under transiently increased metabolic rates in response to insulin.

In conclusion, we present here, to the best of our knowledge, the most comprehensive data-driven dynamic mTOR–AMPK network model. Our combined modelling–experimental approach revealed IRS as a mediator of AMPK induction in response to insulin and strongly suggests an involvement of the mTORC1-dependent NFL in AMPK regulation. The impact of this novel signalling interconnection for AMPK and mTOR biology deserves further exploration. Our findings will be highly relevant to the biomedical field because they can have important implications for administration of drugs targeting mTOR and AMPK, which are commonly used in tumour and metabolic disease treatments.

Materials and methods

Cell lines and lentiviral transduction

Experiments were performed in HeLa α Kyoto cells and C2C12 myocytes. For inducible knockdown of Raptor, HeLa cells were transduced with lentivirus encoding the tetracycline-sensitive tetracycline repressor (tTR)-Krueppel-associated box (protein domain) (KRAB) repressor and a DsRed reporter [50]. Cells were subsequently transfected with lentivirus encoding the Raptor-specific shRNA (target sequence: 5′-GGCTAGTCTGTTTCGAAATTT-3′) and a green fluorescent protein reporter (pLVTH vector), both under the control of tTR-KRAB.

Overexpression of IRS, PTEN and myristoylated Akt variants

N-terminally and hemagglutinin (HA)-tagged pSG5L HA PTEN wt (#10750), N-terminally myristoylated and HA tagged pLNCX.myr.HA.Akt1 (#9005) and N-terminally myristoylated and HA-tagged kinase dead pLNCX.myr.HA.Akt1 K179M (#9006) were ordered from Addgene. IRS1 constructs were a kind gift from A. Tzatsos [36]. Transfection was performed with 6 μg of construct per 6-cm dish using JetPEI reagent according to the manufacturer's instructions. Cells were harvested 24 h after transfection.

Antibodies and reagents

The monoclonal anti-glyceraldehyde-3-phosphate dehydrogenase (GAPDH) IgG1 was purchased from Abcam (Cambridge, UK). The anti-HA IgG 2b k (clone 12CA5) was purchased from Roche. Horseradish peroxidase (HRP)-conjugated goat anti-mouse and goat anti-rabbit IgGs were purchased from Pierce Biotechnology (Thermo Scientific, Rockford, IL USA). All other antibodies were purchased from Cell Signalling Technology (Danvers, MA, USA). Doxycycline for knockdown induction was purchased from Calbiochem, Merck (Darmstadt, Germany). Wortmannin was purchased from Sigma Aldrich (St Louis, MO, USA). Chemicals were supplied by Carl Roth (Karlsruhe, Germany) unless indicated otherwise.

Analysis of cell lysates

Where indicated, HeLa cells were starved for serum and amino acids by exchanging standard growth medium for Hank's balanced salt solution (HBSS) overnight to inhibit mTOR pathway activity. After 16 h of starvation, mTOR signalling was restimulated for 30 min with DMEM containing amino acids and supplemented with 100 nM insulin (Sigma Aldrich).

Gradual knockdown of Raptor was established by induction with 5 μg mL^{-1} of doxycycline (Calbiochem, Merck) for 0, 2 or 3 days. Wortmannin treatment: Wortmannin was added to HBSS 30 min before restimulation for 30 min with Dulbecco's modified Eagle's medium (DMEM), which was supplemented with 100 nM insulin and wortmannin. Cells were washed once with $NaCl/P_i$ and lysed with TNE lysis buffer [50 mM Tris/HCl, pH 8.0, 150 mM NaCl, 1% (v/v) Triton X-100 (Calbiochem, Merck), Complete (Roche, Mannheim, Germany), Phosphatase Inhibitor Cocktail 2 and Phosphatase Inhibitor Cocktail 3 (both Sigma Aldrich)]. Protein concentrations were measured using the Protein Assay Dye Reagent Concentrate (Bio-Rad, Hercules, CA, USA) according to the manufacturer's protocol. Concentrations were adjusted with lysis buffer. Lysates were diluted in sample buffer (5×: 6 mL of glycerol, 0.6 mL of beta-mercaptoethanol, 1.0 g of SDS, 3.75 mL of 1 M Tris, pH 6.8, 2 mg of Bromophenol Blue and 2 mL of H_2O). Whole-cell lysates were analysed using SDS/PAGE. Proteins were transferred to poly(vinylidene difluoride) membranes (Millipore, Billerica, MA, USA), blocked with 5% BSA in TBST (8 g of NaCl, 0.2 g of KCl, 8 g of Tris, pH 7.4, 0.1% Tween 20) for a minimum of 30 min and incubated with the primary antibody in 5% BSA in TBST overnight with shaking at 4°C. Blots were washed 3× with TBST, incubated with secondary antibodies coupled to HRP and washed 3× with TBST before detection.

Modelling

The illustrated graphical model in SBGN graphical notation [51] was designed using CellDesigner 4.2 [52]. The Matlab Toolbox PottersWheel [31] was used for designing and calibrating the models. The parameters for each of the models were estimated by 1000 fits with a parameter disturbance noise of 0.4 using the best fit as the starting value. For each fit a maximum of 250 iterations with χ^2 and parameter tolerances of 1e−07 were run using the optimization algorithm, TrustRegion. To reduce the computation time, cvodes integrator was selected and configured with the following parameters: maximum number of steps = 1500, relative tolerance = 1e−06 and absolute tolerance = 1e−08.

The reactions representing the dynamics of the models were described by mass action laws. Only the kinetic rate constants were estimated, and the interval [1e−06, 1e+04] was selected as constraint for each parameter. The protein initial concentrations were directly determined from our experimental data and scaled to distribute the fitting quality over the model. Experimental error bars indicate SEM. The dynamics for the species PI3K-variant were assumed by reproducing the dynamics of the insulin receptor, whereas its initial concentration was the same of the IRS1 species.

Structural identifiability was calculated *a priori* using GenSSI [32]. The model in Potterswheel format was exported in SBML and converted to Octave format using The System Biology Format Converter (SBFC) (available from sourseforge.net). Then, the model in Octave format was adapted for the software GenSSI. Symbolic solutions for each model were computed, setting 10 as the maximum number of iterations.

After executing each sequence fits, parameters were considered as nonidentifiable when their CV, measured in the best 50% fits of the calibration sequence, were higher than 5%. In combination with this preliminary analysis, the PottersWheel plugin MOTA was used to confirm the parameter nonidentifiability and to assess the relations between the target parameter and the others.

3D sensitivity analysis was performed using PottersWheel and is provided in Fig. S2. We also used PottersWheel to export the models as SBML [53] Level 2 Version 4.

Statistics

The goodness-of-fit statistical measures χ^2 [31], AIC, AICc [34] and BIC [35] were used in order to rank the hypotheses. All these measures were directly computed using PottersWheel Toolbox.

The statistical and programming language R v. 2.13.1 [54] was selected for the graphic representation of the identifiability matrix computed with MOTA.

Acknowledgements

This study was supported by the EC 6th FP NoE LifeSpan (LSHG-CT-2007-036894), the Schlieben-Lange-Programm (K.T.), the Excellence Initiative of the German Federal and State Governments (EXC 294) and the BMBF Gerontosys II – NephAge (031 5896A) (K.T.). We thank A. Tzatsos for kindly providing the IRS1 plasmids. Some of this work is part of a pending European patent application that was filed on 1 June 2011 (Application no. 11004471.6 – 1225). An International Patent Application was filed on 21 March 2012 (number to be assigned).

References

1 Zoncu R, Efeyan A & Sabatini DM (2011) mTOR: from growth signal integration to cancer, diabetes and ageing. *Nat Rev Mol Cell Biol* **12**, 21–35.
2 Polak P & Hall MN (2009) mTOR and the control of whole body metabolism. *Curr Opin Cell Biol* **21**, 209–218.
3 Sengupta S, Peterson TR & Sabatini DM (2010) Regulation of the mTOR complex 1 pathway by nutrients, growth factors, and stress. *Mol Cell* **40**, 310–322.
4 Howell JJ & Manning BD (2011) mTOR couples cellular nutrient sensing to organismal metabolic homeostasis. *Trends Endocrinol Metab* **22**, 94–102.
5 Thedieck K & Hall MN (2009) Translational control by amino acids and energy. In *The Handbook of Cell Signaling* (Bradshaw R & Dennis E eds), pp. 2285–2293. Elsevier, Academic Press, Amsterdam.
6 Thedieck K, Polak P, Kim ML, Molle KD, Cohen A, Jeno P, Arrieumerlou C & Hall MN (2007) PRAS40 and PRR5-like protein are new mTOR interactors that regulate apoptosis. *PLoS One* **2**, e1217.
7 Vander Haar E, Lee SI, Bandhakavi S, Griffin TJ & Kim DH (2007) Insulin signalling to mTOR mediated by the Akt/PKB substrate PRAS40. *Nat Cell Biol* **9**, 316–323.
8 Sancak Y, Thoreen CC, Peterson TR, Lindquist RA, Kang SA, Spooner E, Carr SA & Sabatini DM (2007) PRAS40 is an insulin-regulated inhibitor of the mTORC1 protein kinase. *Mol Cell* **25**, 903–915.
9 Wang L, Harris TE, Roth RA & Lawrence JC Jr (2007) PRAS40 regulates mTORC1 kinase activity by functioning as a direct inhibitor of substrate binding. *J Biol Chem* **282**, 20036–20044.
10 Fonseca BD, Smith EM, Lee VH, MacKintosh C & Proud CG (2007) PRAS40 is a target for mammalian target of rapamycin complex 1 and is required for signaling downstream of this complex. *J Biol Chem* **282**, 24514–24524.

11 Oshiro N, Takahashi R, Yoshino K, Tanimura K, Nakashima A, Eguchi S, Miyamoto T, Hara K, Takehana K, Avruch J *et al.* (2007) The proline-rich Akt substrate of 40 kDa (PRAS40) is a physiological substrate of mammalian target of rapamycin complex 1. *J Biol Chem* **282**, 20329–20339.
12 Wang L, Harris TE & Lawrence JC Jr (2008) Regulation of proline-rich Akt substrate of 40 kDa (PRAS40) function by mammalian target of rapamycin complex 1 (mTORC1)-mediated phosphorylation. *J Biol Chem* **283**, 15619–15627.
13 Dalle Pezze P, Sonntag AG, Thien A, Prentzell MT, Gödel M, Fischer S, Neumann-Haefelin E, Huber TB, Baumeister R, Shanley DP *et al.* (2012) A dynamic network model of mTOR signalling reveals TSC-independent mTORC2 regulation. *Sci Signal* **5**, ra25. doi:10.1126/scisignal.2002469.
14 Mihaylova MM & Shaw RJ (2011) The AMPK signalling pathway coordinates cell growth, autophagy and metabolism. *Nat Cell Biol* **13**, 1016–1023.
15 Lizcano JM, Goransson O, Toth R, Deak M, Morrice NA, Boudeau J, Hawley SA, Udd L, Makela TP, Hardie DG *et al.* (2004) LKB1 is a master kinase that activates 13 kinases of the AMPK subfamily, including MARK/PAR-1. *EMBO J* **23**, 833–843.
16 Hawley SA, Pan DA, Mustard KJ, Ross L, Bain J, Edelman AM, Frenguelli BG & Hardie DG (2005) Calmodulin-dependent protein kinase kinase-beta is an alternative upstream kinase for AMP-activated protein kinase. *Cell Metab* **2**, 9–19.
17 Fogarty S, Hawley SA, Green KA, Saner N, Mustard KJ & Hardie DG (2010) Calmodulin-dependent protein kinase kinase-beta activates AMPK without forming a stable complex: synergistic effects of Ca2+ and AMP. *Biochem J* **426**, 109–118.
18 Hurley RL, Anderson KA, Franzone JM, Kemp BE, Means AR & Witters LA (2005) The Ca2+/calmodulin-dependent protein kinase kinases are AMP-activated protein kinase kinases. *J Biol Chem* **280**, 29060–29066.
19 Woods A, Dickerson K, Heath R, Hong SP, Momcilovic M, Johnstone SR, Carlson M & Carling D (2005) Ca2+/calmodulin-dependent protein kinase kinase-beta acts upstream of AMP-activated protein kinase in mammalian cells. *Cell Metab* **2**, 21–33.
20 Xie M, Zhang D, Dyck JR, Li Y, Zhang H, Morishima M, Mann DL, Taffet GE, Baldini A, Khoury DS *et al.* (2006) A pivotal role for endogenous TGF-beta-activated kinase-1 in the LKB1/AMP-activated protein kinase energy-sensor pathway. *Proc Natl Acad Sci USA* **103**, 17378–17383.
21 Herrero-Martin G, Hoyer-Hansen M, Garcia-Garcia C, Fumarola C, Farkas T, Lopez-Rivas A & Jaattela M (2009) TAK1 activates AMPK-dependent cytoprotective autophagy in TRAIL-treated epithelial cells. *EMBO J* **28**, 677–685.
22 Momcilovic M, Hong SP & Carlson M (2006) Mammalian TAK1 activates Snf1 protein kinase in yeast and phosphorylates AMP-activated protein kinase in vitro. *J Biol Chem* **281**, 25336–25343.
23 Suzuki A, Kusakai G, Kishimoto A, Shimojo Y, Ogura T, Lavin MF & Esumi H (2004) IGF-1 phosphorylates AMPK-alpha subunit in ATM-dependent and LKB1-independent manner. *Biochem Biophys Res Commun* **324**, 986–992.
24 Sun Y, Connors KE & Yang DQ (2007) AICAR induces phosphorylation of AMPK in an ATM-dependent, LKB1-independent manner. *Mol Cell Biochem* **306**, 239–245.
25 Meares GP, Hughes KJ, Naatz A, Papa FR, Urano F, Hansen PA, Benveniste EN & Corbett JA (2011) IRE1-dependent activation of AMPK in response to nitric oxide. *Mol Cell Biol* **31**, 4286–4297.
26 Inoki K, Zhu T & Guan KL (2003) TSC2 mediates cellular energy response to control cell growth and survival. *Cell* **115**, 577–590.
27 Gwinn DM, Shackelford DB, Egan DF, Mihaylova MM, Mery A, Vasquez DS, Turk BE & Shaw RJ (2008) AMPK phosphorylation of raptor mediates a metabolic checkpoint. *Mol Cell* **30**, 214–226.
28 Polak P, Cybulski N, Feige JN, Auwerx J, Ruegg MA & Hall MN (2008) Adipose-specific knockout of raptor results in lean mice with enhanced mitochondrial respiration. *Cell Metab* **8**, 399–410.
29 Aguilar V, Alliouachene S, Sotiropoulos A, Sobering A, Athea Y, Djouadi F, Miraux S, Thiaudiere E, Foretz M, Viollet B *et al.* (2007) S6 kinase deletion suppresses muscle growth adaptations to nutrient availability by activating AMP kinase. *Cell Metab* **5**, 476–487.
30 Inoki K, Ouyang H, Li Y & Guan KL (2005) Signaling by target of rapamycin proteins in cell growth control. *Microbiol Mol Biol Rev* **69**, 79–100.
31 Maiwald T & Timmer J (2008) Dynamical modeling and multi-experiment fitting with PottersWheel. *Bioinformatics* **24**, 2037–2043.
32 Chis O, Banga JR & Balsa-Canto E (2011) GenSSI: a software toolbox for structural identifiability analysis of biological models. *Bioinformatics* **27**, 2610–2611.
33 Hengl S, Kreutz C, Timmer J & Maiwald T (2007) Data-based identifiability analysis of non-linear dynamical models. *Bioinformatics* **23**, 2612–2618.
34 Akaike H (1974) A new look at the statistical model identification. *IEEE Trans Automat Contr* **19**, 716–723.
35 Schwarz G (1978) Estimating the dimension of a model. *Ann Stat* **6**, 461–464.
36 Tzatsos A & Kandror KV (2006) Nutrients suppress phosphatidylinositol 3-kinase/Akt signaling via raptor-dependent mTOR-mediated insulin receptor substrate 1 phosphorylation. *Mol Cell Biol* **26**, 63–76.
37 Kohn AD, Takeuchi F & Roth RA (1996) Akt, a pleckstrin homology domain containing kinase, is activated

primarily by phosphorylation. *J Biol Chem* **271**, 21920–21926.
38 Caron E, Ghosh S, Matsuoka Y, Ashton-Beaucage D, Therrien M, Lemieux S, Perreault C, Roux PP & \Kitano H (2010) A comprehensive map of the mTOR signaling network. *Mol Syst Biol* **6**, 453.
39 Sedaghat AR, Sherman A & Quon MJ (2002) A mathematical model of metabolic insulin signaling pathways. *Am J Physiol Endocrinol Metab* **283**, E1084–E1101.
40 Jain P & Bhalla US (2009) Signaling logic of activity-triggered dendritic protein synthesis: an mTOR gate but not a feedback switch. *PLoS Comput Biol* **5**, e1000287.
41 Faratian D, Goltsov A, Lebedeva G, Sorokin A, Moodie S, Mullen P, Kay C, Um IH, Langdon S, Goryanin I *et al.* (2009) Systems biology reveals new strategies for personalizing cancer medicine and confirms the role of PTEN in resistance to trastuzumab. *Cancer Res* **69**, 6713–6720.
42 Vinod PK & Venkatesh KV (2009) Quantification of the effect of amino acids on an integrated mTOR and insulin signaling pathway. *Mol BioSyst* **5**, 1163–1173.
43 Borisov N, Aksamitiene E, Kiyatkin A, Legewie S, Berkhout J, Maiwald T, Kaimachnikov NP, Timmer J, Hoek JB & Kholodenko BN (2009) Systems-level interactions between insulin-EGF networks amplify mitogenic signaling. *Mol Syst Biol* **5**, 256.
44 Kuepfer L, Peter M, Sauer U & Stelling J (2007) Ensemble modeling for analysis of cell signaling dynamics. *Nat Biotechnol* **25**, 1001–1006.
45 Kiselyov VV, Versteyhe S, Gauguin L & De Meyts P (2009) Harmonic oscillator model of the insulin and IGF1 receptors' allosteric binding and activation. *Mol Syst Biol* **5**, 243.
46 Ning J & Clemmons DR (2010) AMP-activated protein kinase inhibits IGF-I signaling and protein synthesis in vascular smooth muscle cells via stimulation of insulin receptor substrate 1 S794 and tuberous sclerosis 2 S1345 phosphorylation. *Mol Endocrinol* **24**, 1218–1229.
47 Tzatsos A & Tsichlis PN (2007) Energy depletion inhibits phosphatidylinositol 3-kinase/Akt signaling and induces apoptosis via AMP-activated protein kinase-dependent phosphorylation of IRS-1 at Ser-794. *J Biol Chem* **282**, 18069–18082.
48 Jakobsen SN, Hardie DG, Morrice N & Tornqvist HE (2001) 5′-AMP-activated protein kinase phosphorylates IRS-1 on Ser-789 in mouse C2C12 myotubes in response to 5-aminoimidazole-4-carboxamide riboside. *J Biol Chem* **276**, 46912–46916.
49 Garcia-Echeverria C (2011) Blocking the mTOR pathway: a drug discovery perspective. *Biochem Soc Trans* **39**, 451–455.
50 Wiznerowicz M & Trono D (2003) Conditional suppression of cellular genes: lentivirus vector-mediated drug-inducible RNA interference. *J Virol* **77**, 8957–8961.
51 Le Novere N, Hucka M, Mi H, Moodie S, Schreiber F, Sorokin A, Demir E, Wegner K, Aladjem MI, Wimalaratne SM *et al.* (2009) The Systems Biology Graphical Notation. *Nat Biotechnol* **27**, 735–741.
52 Funahashi A, Morohashi M, Kitano H & Tanimura N (2003) CellDesigner: a process diagram editor for gene-regulatory and biochemical networks. *BIOSILICO* **1**, 159–162.
53 Hucka M, Finney A, Sauro HM, Bolouri H, Doyle JC, Kitano H, Arkin AP, Bornstein BJ, Bray D, Cornish-Bowden A *et al.* (2003) The systems biology markup language (SBML): a medium for representation and exchange of biochemical network models. *Bioinformatics* **19**, 524–531.
54 R Development Core Team (2005) *A Language and Environment for Statistical Computing*. R Foundation for Statistical Computing, Vienna, Austria.

Supporting information

The following supplementary material is available:
Fig. S1. Identifiability and parameter estimation for the IR-beta-induced AMPK model (hypothesis No.2).
Fig. S2. Sensitivity analysis for the IRS1-induced AMPK model (hypothesis No.3).
Fig. S3. Additional simulated versus experimental time courses for the IRS1-induced AMPK model (hypothesis No.3).
Model S1. febs_mtor_model_ampk_by_irs1_pottersWheel.m (PottersWheel format).
Model S2. febs_mtor_model_ampk_by_irs1_sbml.xml (SBML format).

This supplementary material can be found in the online version of this article.

Please note: As a service to our authors and readers, this journal provides supporting information supplied by the authors. Such materials are peer-reviewed and may be reorganized for online delivery, but are not copy-edited or typeset. Technical support issues arising from supporting information (other than missing files) should be addressed to the authors.